APPLIED PHYSICS LETTERS **89**, 124101 (2006)

Array-compatible transition-edge sensor microcalorimeter γ-ray detector with 42 eV energy resolution at 103 keV

B. L. Zink, J. N. Ullom, J. A. Beall, K. D. Irwin, W. B. Doriese, W. D. Duncan, L. Ferreira, G. C. Hilton, R. D. Horansky, C. D. Reintsema, and L. R. Vale[a)]
National Institute of Standards and Technology, 325 Broadway MC 817.03, Boulder, Colorado 80305

(Received 11 March 2006; accepted 21 July 2006; published online 20 September 2006)

The authors describe a microcalorimeter γ-ray detector with measured energy resolution of 42 eV full width at half maximum for 103 keV photons. This detector consists of a thermally isolated superconducting transition-edge thermometer and a superconducting bulk tin photon absorber. The absorber is attached with a technique compatible with producing arrays of high-resolution γ-ray detectors. The results of a detailed characterization of the detector, which includes measurements of the complex impedance, detector noise, and time-domain pulse response, suggest that a deeper understanding and optimization of the thermal transport between the absorber and thermometer could significantly improve the energy resolution of future detectors. [DOI: 10.1063/1.2352712]

Low temperature microcalorimeters and microbolometers represent the state of the art in photon detection over a wide range of wavelengths.[1] For example, microcalorimeters based on superconducting transition-edge sensors (TESs), which can measure the energy of x rays in the 6 keV regime to within 2.4 eV, have potential uses for x-ray astronomy and x-ray microanalysis.[2] For some time, researchers have realized the potential of TES microcalorimeters for measuring hard x-ray and γ radiations, where a bulk absorber is required for sufficient absorption efficiency. Previous work has demonstrated that attaching superconducting bulk tin absorbers to TES microcalorimeters provides a potential route to high-resolution γ-ray detectors,[3] but higher energy resolution and the implementation of arrays of detectors are necessary for the most promising applications, which include passive, nondestructive assay of nuclear materials such as plutonium isotopic mixtures[4] and spent uranium fuel assemblies,[5] and precise determination of the Lamb shift in heavy hydrogenlike atoms.[6]

In this letter we present experimental results obtained with a composite microcalorimeter in which the thermometer is an optimized, voltage-biased, Mo/Cu TES and photons are absorbed in a superconducting bulk tin slab. The γ-ray spectra show an energy resolution of 42 eV full width at half maximum (FWHM) at 103 keV, more than an order of magnitude better than typical high-resolution γ-ray detectors. We also characterize the detector by comparing measurements of the TES complex impedance Z_{TES}, current noise I_n, small-signal pulse response, and energy resolution to the predictions of thermal models. Our results suggest that a deeper understanding of the thermal transport in the device could lead to further improvement in energy resolution.

Figure 1(a) is an optical micrograph of the composite microcalorimeter. The design of the Mo/Cu TES, which is thermally isolated from the bulk Si substrate with a silicon-nitride (Si–N) membrane, is described elsewhere.[7] We patterned a 150 μm diameter, 20 μm tall post on the TES using a negative photoresist and coated the top face with a thin layer of glue. We then cut a 250 μm thick sheet of high-purity cold-rolled Sn into a 900–950 μm square, aligned the TES and post to this absorber, and mated them to form a composite microcalorimeter with estimated quantum efficiency of 25% for 100 keV photons. This technique allows arrays of composite microcalorimeters to be assembled in a single gluing step. Figure 1(b) shows a 16 pixel composite TES γ-ray detector array that we are currently testing using a time-division superconducting quantum interference device (SQUID) multiplexer. The energy spectrum of a ^{153}Gd calibration source measured with the TES voltage biased such that the equilibrium resistance, $R_0 = 0.25R_n$ (normal state resistance $R_n = 8.3\ \mathrm{m}\Omega$), appears in Fig. 1(c).

The simplest thermal model of a composite microcalorimeter appears in Fig. 1(d). C_a represents the heat capacity of the absorber, which is linked to the TES heat capacity C_{TES} via a thermal conductance G_a. Heat flow from the TES to the bath at T_b is largely through the Si–N membrane,

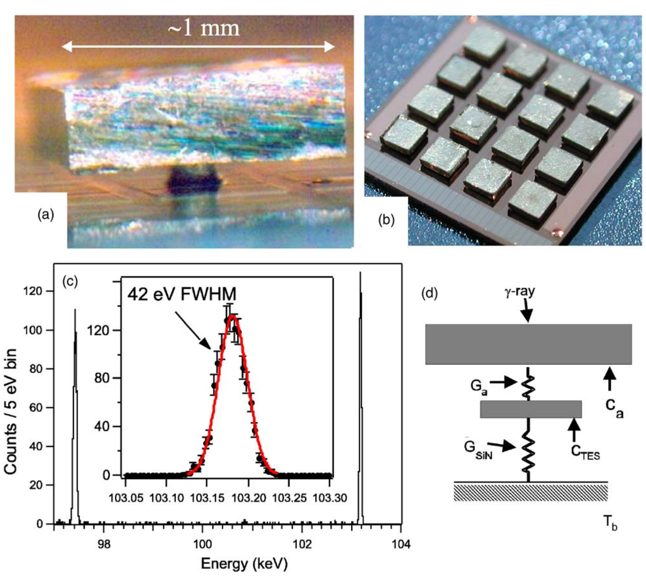

FIG. 1. (Color online) (a) Side-view optical micrograph of the composite TES microcalorimeter. (b) A 16 pixel composite TES array. (c) Spectrum of optimally filtered and drift-corrected pulse heights from ^{153}Gd, with lines at 97 and 103 keV. The inset graph shows the 103 keV peak, where the solid line is a least-squares Gaussian fit with $\Delta E_{\mathrm{FWHM}} = 42$ eV. A simple scaling predicts that a similar detector with 4 mm^2 collection area would have $\Delta E_{\mathrm{FWHM}} \sim 84$ eV. (d) Thermal model of the composite microcalorimeter.

[a)]Electronic mail: bzink@boulder.nist.gov

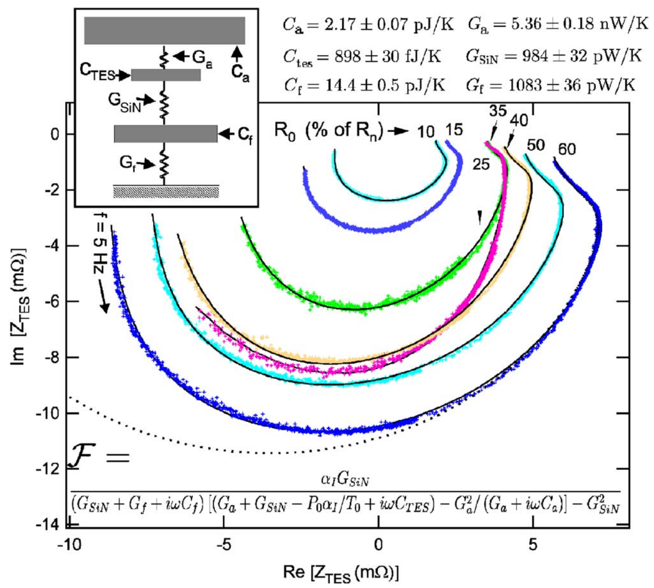

FIG. 2. (Color online) Parametric plot of Re$[Z_{TES}]$ vs Im$[Z_{TES}]$ from 5 to 5000 Hz. Solid lines are fits to $Z_{TES}=R_0(1+\beta_I)+R_0(2+\beta_I)(P_0/T_0)\mathcal{F}$, where $\mathcal{F}$ is the function of α_I and the thermal parameters of the model shown in the figure. P_0 is the equilibrium power dissipated in the TES. The single dotted line is the prediction of the thermal model with no C_f and G_f for $R_0=0.60R_n$ and the other parameters fixed.

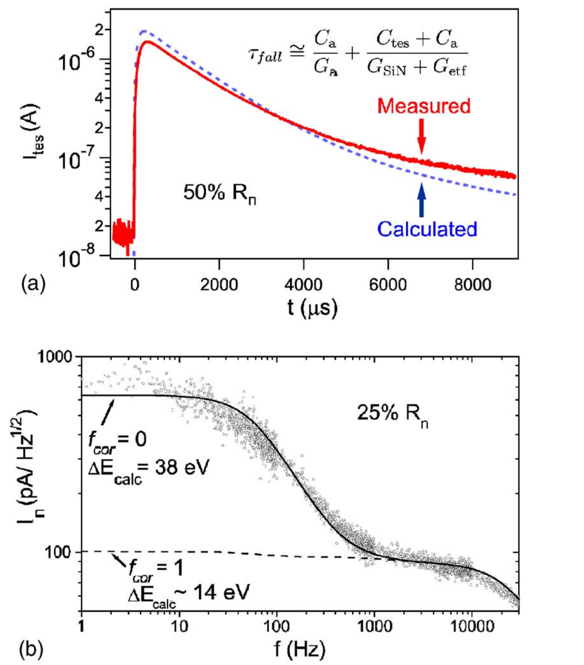

FIG. 3. (Color online) (a) Small-signal pulse response for $R_0=0.5R_n$. Solid line is the measured response of the TES to 5.9 keV x-ray pulses, dashed line shows calculated response determined using fit parameters from Z_{TES}. Measured $\tau_{fall}=1.302\pm0.012$ ms, calculated $\tau_{fall}=1.30$ ms, and the value estimated from the simple equation displayed is $\tau_{fall}\sim1.40$ ms. (b) I_n vs f. Lines are calculated from Eq. (1) with $\Gamma=1.66$.

represented by G_{SiN}. This model is described by three coupled differential equations. We determine the expressions for Z_{TES} and I_n used below by extending the formalism presented by Irwin and Hilton[8] to the composite microcalorimeter in the small-signal limit.

The complex impedance of the voltage-biased TES circuit is the current response to a frequency-dependent voltage added to the bias voltage, $Z(\omega)=\delta V/\delta I=R_L+i\omega L+Z_{TES}$, where R_L is the effective load resistance, and L is the self-inductance of the input coil of the SQUID amplifier which measures δI.[8] Measurements of Z_{TES} provide a powerful tool for characterizing TES microcalorimeters.[9,10] Figure 2 plots Im$[Z_{TES}]$ vs Re$[Z_{TES}]$ measured for a series of bias voltages at $T_b=80$ mK. For a simple calorimeter, Z_{TES} traces a semicircle on this plot. The data in Fig. 2 deviate from this behavior in two ways: a bulge appears in the higher f region due to C_a and G_a, and a low-f shift requires the presence of a third C and G, as shown in the inset of Fig. 2.

This three-body thermal model introduces an additional thermal impedance between the TES, which is the center pixel of a small TES array, and the heat bath. Heat flowing from the TES travels through the Si–N membrane to an intermediate heat capacity, C_f, formed by the Si frame supporting the pixel. Heat then flows from the frame along the Si bars to the exterior of the Si chip held at T_b via the thermal conductance G_f. C_f and G_f add a fourth differential equation to the system and appear in the predicted equation for Z_{TES} given in Fig. 2. Note that each term in the numerator and denominator of $\mathcal{F}$ contains exactly two of the fit parameters. This means multiplying all C's, all G's, and α_I by the same factor gives the same fit. Therefore, a separate measurement of one or more of these parameters is required to extract meaningful values from the fit. Measurements of the TES *I-V* curve allow calculation of the power dissipated at a given T, which gives $dP/dT=G_{dc}=(1/G_{SiN}+1/G_f)^{-1}=514\pm17$ pW/K. The fit parameters in the upper inset of Fig. 2 are averages of fit results for all bias points and are in reasonable agreement with values of heat capacity and thermal conductivity available in the literature. The resulting α_I varies nonmonotonically with R_0 from 14 to 50, while β_I shows a general trend from 1.1 to 0.1 with increasing R_0. Using these parameters we can calculate the expected behavior of I_n and small-signal pulse response and compare to values measured at the same T_b and on the same cooling cycle as the Z_{TES} data shown in Fig. 2.

Figure 3(a) shows the measured current response of the TES to a 5.9 keV x ray, with the predicted time-domain response calculated by numeric solution of the coupled electrothermal differential equations. These calculations give a fall time which agrees well with the measured τ_{fall} of small-signal pulses. Conversely the calculated rise time τ_{rise} significantly underestimates the measured values ($\tau_{rise}=111\pm4$ μs). Figure 3(a) also includes a simple approximate expression for the small-signal fall time in the limit of small L, $R_L \ll R_0$, and $G_{SiN}<G_a$ that also roughly agrees with the measured τ_{fall}. A further departure from expected behavior is a second, $\sim$10 ms time-constant apparent in the measured pulse. This long athermal tail also appears in γ-ray pulses and has been reported in other composite microcalorimeters.[11] These effects could be due to interactions between phonons and photon-generated quasiparticles that are absent from the model. We are currently designing experiments to more carefully probe the physics of the absorber.

Figure 3(b) shows the measured I_n for $R_0=0.25R_n$. Although calculations using the three-body model give slightly better agreement, for simplicity we use the two-body thermal model with $G_{SiN}=G_{dc}$. To calculate $I_n=\sqrt{S_I}$ we use the nonlinear equilibrium ansatz,[8] which has been shown to be rigorous for small deviations from equilibrium,[12] and write

$$S_I(\omega) = |Y^I_{1,1}|^2 \frac{S_{V_{\rm int}}}{L^2} + |Y^I_{1,2}|^2 \frac{S_{P_a}}{C_a^2} + |Y^I_{1,3}|^2 \frac{S_{P_{\rm SiN}}}{C_{\rm TES}^2}, \qquad (1)$$

where $S_{V_{\rm int}} = 4k_b T_0 R_0 \xi(I_0)(1+\Gamma^2)$, $\xi(I_0) \cong 1 + 2\beta_I$, $S_{P_a} = 4k_b T_0^2 G_a$, $S_{P_{\rm SiN}} = 4k_b T_0^2 G_{\rm SiN}$, $Y^I_{i,j} = (Z_I^{-1})_{i,j}$, and Z_I is a matrix that describes the T and I response to internal power fluctuations,[8]

$$Z_I = \begin{bmatrix} \frac{R_L + R_0(1+\beta_I)}{L} + i\omega & 0 & \frac{P_0\alpha_I}{I_0 T_0 L} \\ 0 & \frac{G_a}{C_a} + i\omega & -G_a/C_a \\ -\frac{I_0(R_L - R_0) + i\omega L I_0}{C_{\rm TES}} & -\frac{G_a + A(i\omega C_a + G_a)}{C_{\rm TES}} & \frac{G_a(1+A) + G_{\rm SiN}}{C_{\rm TES}} + i\omega \end{bmatrix}. \qquad (2)$$

Here $A = (1 - 2f_{\rm cor})$, and $f_{\rm cor}$ is an adjustable parameter ($0 \leqslant f_{\rm cor} \leqslant 1$) that controls the degree of correlation between the power flowing out of the absorber and the power flowing into the TES. $Y^I_{i,j}$ therefore depend on $f_{\rm cor}$ and are most easily determined numerically. The adjustable parameter $\Gamma = 1.66$ characterizes the typical "excess" or "unexplained" out-of-band TES noise[7,8] and was determined by χ^2 minimization.

The dashed line in Fig. 3(b) is the prediction of the model with $f_{\rm cor} = 1$, which is the energy-conserving case. The low value at low f is a result of the correlation between noise power at either end of G_a. The actual noise of the detector significantly exceeds this prediction and is best described by the $f_{\rm cor} = 0$ case, where the noise power at either end of G_a is uncorrelated. This suggests that the thermal transport from the absorber to the TES is more complicated than the simple lumped-element model predicts, and that the system is non-Markovian. The transport could perhaps be described by a more physical but mathematically cumbersome model that replaces G_a with a large collection of small C's and corresponding G's.[13] The introduction of $f_{\rm cor}$ allows us to use the simple but physically incorrect model as a tool to characterize the detector. We calculate expected optimally filtered energy resolution, $\Delta E_{\rm calc}$ by numerically integrating the results of Fig. 3(b).[14] With $f_{\rm cor} = 0$, $\Delta E_{\rm calc} = 38$ eV, in good agreement with the measured $\Delta E_{\rm FWHM}$. Using $f_{\rm cor} = 1$ gives $\Delta E_{\rm calc} \cong 14$ eV. This $f_{\rm cor} = 1$ calculation suggests that understanding and improving the thermal transport between the absorber and the TES could lead to improvements in $\Delta E_{\rm FWHM}$ of up to a factor of 3.

In summary, we presented γ-ray spectra with $\Delta E_{\rm FWHM} = 42$ eV measured with a TES microcalorimeter with an ~ 1 mm^2 Sn absorber. We also characterized the detector by measuring $Z_{\rm TES}$, I_n, and small-signal pulse response and used the results to compare predicted ΔE with measured values. Our current work is focused on understanding the physics behind $f_{\rm cor}$ and the athermal behavior of the absorber and on demonstrating arrays of TES microcalorimeter γ-ray detectors.

The authors thank M. Rabin, M. Smith, C. Rudy, D. Vo, A. Hoover, and T. Saab for helpful discussions and other contributions and acknowledge the support of the DOE-NNSA and the NIST-EEEL Director's Reserve.

[1] *Cryogenic Particle Detection*, Topics in Applied Physics Vol. 99, edited by C. Enss (Springer, Berlin, 2005).
[2] J. N. Ullom, J. A. Beall, W. B. Doriese, W. D. Duncan, L. Ferreira, G. C. Hilton, K. D. Irwin, C. D. Reintsema, and L. R. Vale, Appl. Phys. Lett. **87**, 194103 (2005).
[3] D. T. Chow, A. Loshak, M. L. van den Berg, M. Frank, T. W. Barbee, Jr., and S. E. Labov, Proc. SPIE **4141**, 67 (2000).
[4] O. B. Drury, S. F. Terracol, and S. Friedrich, Phys. Status Solidi C **2**, 1468 (2005).
[5] J. N. Ullom, B. L. Zink, J. A. Beall, W. B. Doriese, W. D. Duncan, L. Ferreira, G. C. Hilton, K. D. Irwin, C. D. Reintsema, L. R. Vale, M. W. Rabin, A. Hoover, C. R. Rudy, M. K. Smith, D. M. Tournear, and D. T. Vo, IEEE Nuclear Science Symposium, 2005 (unpublished).
[6] A. Bleile, P. Egelhof, H. J. Kluge, U. Liebisch, D. McCammon, H. J. Meier, O. Sebastian, C. K. Stahle, and M. Weber, Nucl. Instrum. Methods Phys. Res. A **444**, 488 (2000).
[7] J. N. Ullom, W. B. Doriese, G. C. Hilton, J. A. Beall, S. Deiker, W. D. Duncan, L. Ferreira, K. D. Irwin, C. D. Reintsema, and L. R. Vale, Appl. Phys. Lett. **84**, 4206 (2004).
[8] K. D. Irwin and G. C. Hilton, in *Cryogenic Particle Detection*, Topics in Applied Physics Vol. 99, edited by C. Enss (Springer, Berlin, 2005), pp. 63–149.
[9] M. A. Lindeman, S. Bandler, R. P. Brekosky, J. A. Chervenak, E. Figueroa-Feliciano, F. M. Finkbeiner, M. J. Li, and C. A. Kilbourne, Rev. Sci. Instrum. **75**, 1283 (2004).
[10] M. Galeazzi and D. McCammon, J. Appl. Phys. **93**, 4856 (2003).
[11] M. L. van den Berg, D. T. Chow, A. Loshak, M. F. Cunningham, T. W. Barbee, Jr., M. A. Frank, and S. E. Labov, Proc. SPIE **4140**, 436 (2000).
[12] K. D. Irwin, Nucl. Instrum. Methods Phys. Res. A **559**, 718 (2006).
[13] J. M. Gildemeister, A. T. Lee, and P. L. Richards, Appl. Opt. **40**, 6229 (2001).
[14] S. H. Moseley, J. C. Mather, and D. McCammon, J. Appl. Phys. **56**, 1257 (1984).